Structure–mechanics relationship of hybrid polyvinyl alcohol-collagen composite by molecular dynamics simulations

Junbo Zhou and Zhao Qin*

Polyvinyl alcohol (PVA) is a water-soluble synthetic polymer that can be used to make hydrogels for biomedical applications as well as biodegradable bags and films; however, compared to other plastics currently used for containers, it lacks mechanical strength, thermal stability, and can easily absorb water from humid environments. Although mechanical improvement has been observed by blending PVA with collagen in a hybrid hydrogel, there is a lack of fundamental understanding of the molecular mechanism, and it is not clear whether the improvement is limited to a hydrated state. Here, using classical molecular dynamics simulations based on fully atomistic models, we develop the equilibrated molecular structure of PVA with collagen and characterize its mechanics. We show that by interacting with a collagen molecule, PVA is equilibrated to a more ordered structure with each residue interacting with the near neighbors by forming more hydrogen bonds locally, making the structure stiffer than pure PVA. The structure shows higher thermal stability before melting, as well as higher rigidity in water. Our results provide the mechanism of the mechanical advantages of hybrid PVA-collagen polymer. The study demonstrates that the structure and mechanics of a synthetic polymer can be tuned by a tiny amount of a natural polymer at the molecular interface. Moreover, it may shed light on identifying a way to improve the mechanics of biodegradable polymer materials without adding much cost, which is crucial for environmental safety.

Impact statement

Blending natural and synthetic polymers (e.g., polyvinyl alcohol [PVA] and collagen in a hybrid hydrogel) has shown advantages in polymer mechanics, but there is a lack of fundamental understanding. Using molecular dynamics (MD) simulations based on fully atomistic models, we develop the equilibrated structure of the PVA with collagen and characterize its mechanics. We show that by interacting with a collagen molecule, PVA is equilibrated to a more ordered structure with each residue interacting with the near neighbors by forming more H-bonds locally and the structure is stiffer than pure PVA. Moreover, the structure shows a higher thermal stability before the melting point of PVA, as well as higher rigidity in water. Our results demonstrate that the structure and mechanics of a synthetic polymer can be tuned by a tiny amount of a natural polymer at the molecular interface. It provides the mechanism of the mechanical advantages as experimentally observed. This study paves the way for the multiscale modeling and mechanical design of the hybrid polymer material. It sheds light on identifying a way to improve the mechanics of biodegradable materials without adding much cost for both material functionality and environmental safety.

Introduction

Plastic (e.g., polyethylene, polyvinyl chloride), though once considered a miracle material with its durability and malleability, now poses a significant environmental threat because of its massive application to single-use products and its difficulty to break down in nature. In 2016 alone, the United States generated 42 million tons of plastic trash, and around 2 million tons were mismanaged, often ending up in rivers and oceans.[1] These materials are slow to break down in nature. For example, conventional polyethylene bags lose less than 2% of their total surface area after 40 weeks at sea.[2] Plastics can accumulate over time and jeopardize the survival of marine animals by affecting their locomotion and reducing their sensation to feed.[3] For instance, plastic bags are often mistaken for food by sea turtles feeding on jellyfish (**Figure 1**). Floating plastics moving with ocean currents can carry invasive species, including barnacles and bryozoans,

Junbo Zhou, Laboratory for Multiscale Material Modeling, Syracuse University, Syracuse, USA; Department of Civil and Environmental Engineering, Syracuse University, Syracuse, USA; Shanghai North America International School, Shanghai, China; Zhao Qin, Laboratory for Multiscale Material Modeling, Syracuse University, Syracuse, USA; Department of Civil and Environmental Engineering, Syracuse University, Syracuse, USA; zqin02@syr.edu
*Corresponding author
doi:10.1557/s43577-022-00416-0

that can be disastrous for local biodiversity.[4,5] While some so-called biodegradable plastics are available for sale, they may need a long time (180 days[6]) and compost facilities to break down.[6] Compost facilities require huge land space near the city, as well as energy and water input for ideal temperature and humidity, limiting the application of this solution. This creates the urgency of an innovative polymer with better biodegradability and sufficient mechanical strength.

A few water-soluble synthetic polymers make it possible to create highly biodegradable materials.[7–10] Many of these polymers are produced from petroleum such as polyethylene glycol, polyvinyl alcohol (PVA), poly(*N*-isopropylacrylamide), polyacrylamide, and polyvinylpyrrolidone. They have biomedical applications (e.g., implant, drug delivery, and scaffold) because they can form hydrogels with good biocompatibility.[11–14] These polymers appear only in recent decades but many of them show promising and advanced functions. Unlike many biological polymers that have their secondary, tertiary, and higher-order structures well characterized by their revealed related functions, most of the synthetic polymers are only defined by their primary chemical structure of the building block, making their structure–function relations far less understood.[15,16] One of our recent works shows that by annealing PVA hydrogels, their crystallinity as well as their mechanical toughness can be increased.[17] There is evidence to suggest that beyond chemical composition and molecular weight, the higher-order structure, defined by how the chains interact and entangle, can play an important role in defining material functions.[17]

PVA, as a water-soluble synthetic polymer, can be used to make nontoxic bags and films that break down rapidly,[18] but it lacks thermal stability and tolerance to humidity. It is crucial to improve the mechanics of the material in an ambient environment. Many recent studies investigate the mechanics of PVA hydrogel for biomedical applications. Some show that the mechanics (e.g., stiffness and strength) of the PVA hydrogel can be improved by blending PVA and collagen.[19–21] It provides a possible way to improve the mechanics of PVA material; however, there is a lack of fundamental understanding of the molecular mechanism, and it is not clear whether the improvement is limited to a hydrated state of PVA. Actually, there is little research on the theoretical, nanoscale study of the PVA structure,[17,22] which serves as the foundation for a physical understanding of its material functions.

We were thus motivated to investigate the large-scale molecular structures of a PVA-collagen interface and reveal its structure-mechanics relationship. Instead of experimental characterization, which is highly limited by the access to imaging facilities, fully atomistic molecular dynamics (MD) modeling provides a useful tool to predict the PVA-collagen molecular structures in different environments and reveal their material functions by simulating the external loading force and study its mechanical response *in silico*. The nonreactive predefined force field (i.e., CHARMM general force field[23–26] for the current work) greatly reduces the computational complexity from a first-principles-based method and allows us to simulate the relaxation and deformation of such large molecular structures for a sufficient amount of time. The accuracy of the method has been examined against experiments of biopolymers.[27] Recent development of homology and machine learning-based methods has shown advantages in structure prediction,[28,29] but their applications are mainly restricted to protein because there are few ground-truth structures available for synthetic polymers, making MD still a powerful predictive tool. Beyond atomistic structures, coarse-grained models can be further developed based on the atomistic results for material structures at an even larger scale.[30,31]

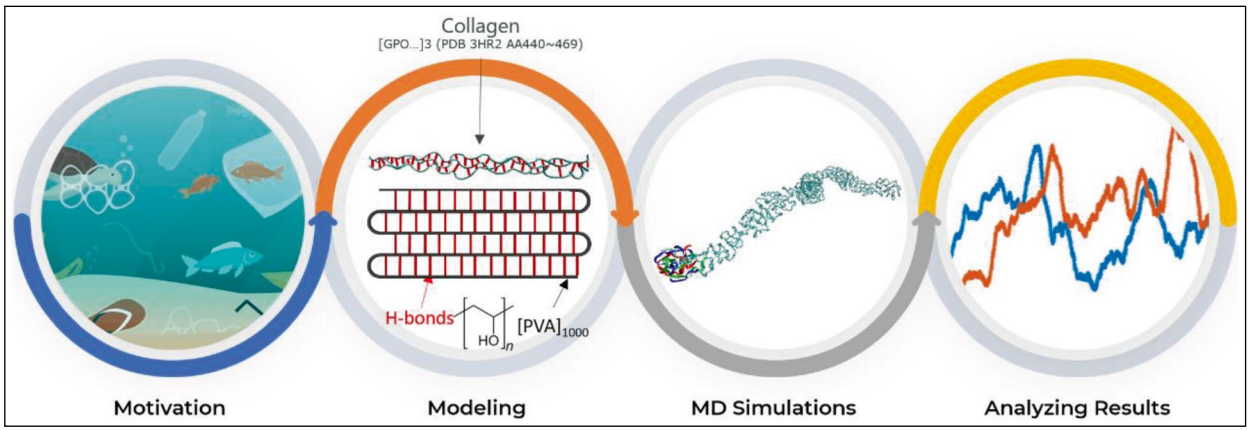

Figure 1. Brief summary of research progression. Motivations: Seeing the dangers of plastic pollution, the need for a strong, durable, and easily degradable material to replace plastic is recognized. Modeling: An unrelaxed PVA-collagen model is created by placing collagen at one end of a PVA straight chain. The PVA chain studied contains 1000 residues. Molecular dynamics (MD) simulations: Chemistry at HARvard Macromolecular Mechanics (CHARMM) general force field is applied to relax or stretch the molecules at desired temperatures, with or without water. Analyzing results: The hydrogen bonding, dihedral angle, end-to-end distance, and force–displacement data generated in the simulation are compiled, visualized, and interpreted.

Methods

We used molecular dynamics, with the general research procedure summarized in Figure 1.

Initial structure of PVA and PVA-collagen molecules

We started by creating a computer model of the molecule of interest. The tropocollagen molecule has a sequence of [GPOGAVGPAGKDGEAGAQGAOGPAGPAGER]$_3$, with each chain composed of 30 amino acids as a section of the full-length collagen of mammalian connective tissues.[32] The major part of the initial molecular model of collagen was obtained from a protein data bank with PDB ID 3HR2 and corresponded to the amino acid 440 to 469 in the original full-length collagen. The two ends were terminated by acetylated N-terminus and N-methylamide C-terminus with zero charge, respectively. A straight chain of PVA backbone could be obtained with an Octave script generating carbon atoms in a set pattern. Using Psfgen[33] with a topology file for protein and PVA,[34] which provides default internal coordinates used to guess the location of atoms, the missing atoms were filled onto the backbone, creating a fully extended PVA straight chain. The particular PVA chain involved in the study consists of 1000 residues with a length of 2594 Å. We assembled the PVA-collagen molecules by placing the collagen molecule close to one end of the PVA straight chain, as illustrated in the upper part of **Figure 2**b.

Relaxation of the molecule in MD simulation

After the models of the molecules are created, the next step was relaxing the molecule in fully atomistic MD simulations. We ran MD simulations with a NAMD package version 2.14.[33] Figure 2a–b show the molecular structure of the 1000-residue PVA molecule and the assembled PVA-collagen molecules before and after relaxation, respectively. The test molecules were relaxed using molecular dynamics simulations first in vacuum with interatomic interactions defined by a CHARMM general force field.[17,35] Simulations for relaxing the structures in vacuum were run at a constant room temperature (300 K) by means of temperature reassignment for every 2 ps, and the relaxed structures were used as starting conformation in

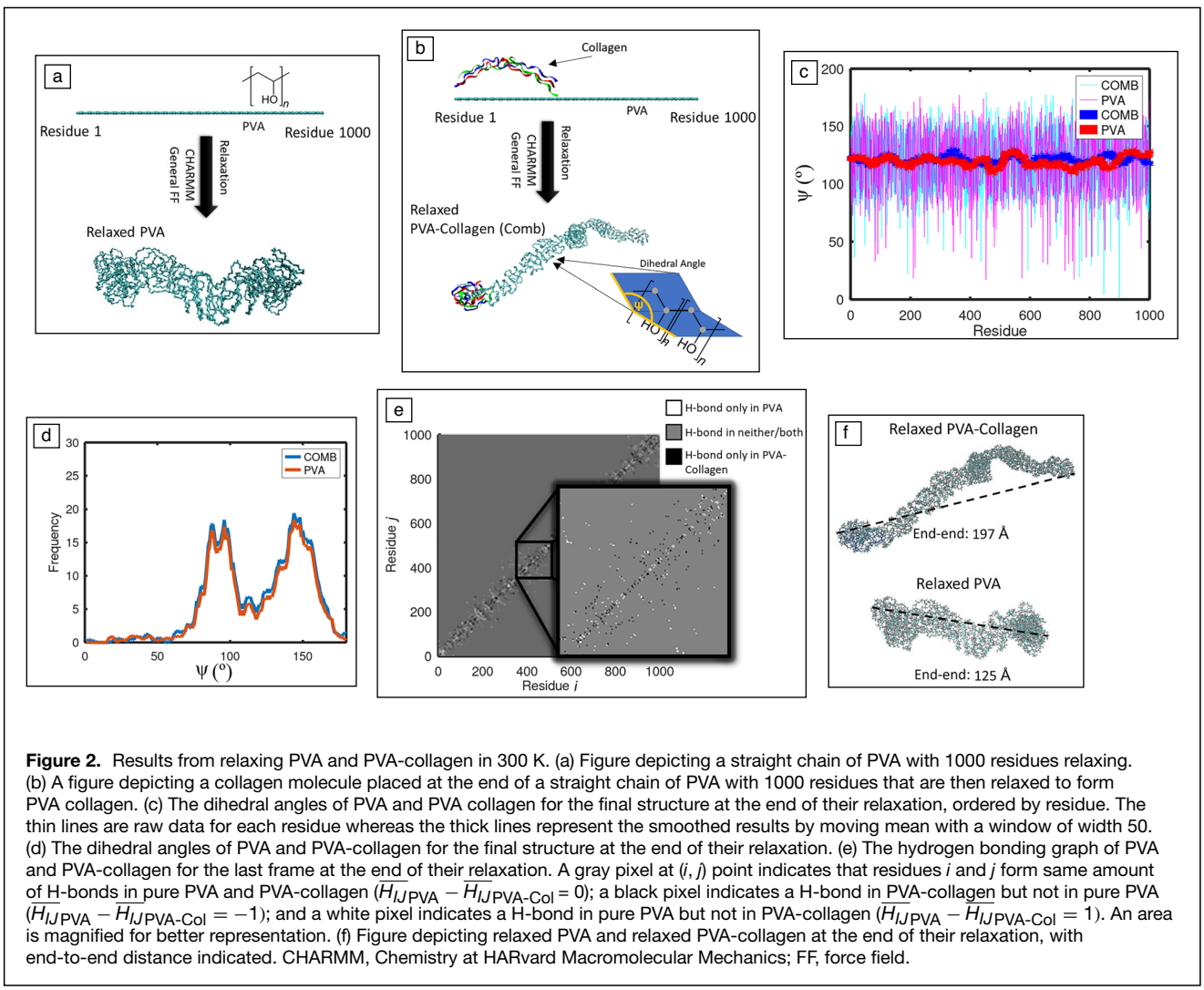

Figure 2. Results from relaxing PVA and PVA-collagen in 300 K. (a) Figure depicting a straight chain of PVA with 1000 residues relaxing. (b) A figure depicting a collagen molecule placed at the end of a straight chain of PVA with 1000 residues that are then relaxed to form PVA collagen. (c) The dihedral angles of PVA and PVA collagen for the final structure at the end of their relaxation, ordered by residue. The thin lines are raw data for each residue whereas the thick lines represent the smoothed results by moving mean with a window of width 50. (d) The dihedral angles of PVA and PVA-collagen for the final structure at the end of their relaxation. (e) The hydrogen bonding graph of PVA and PVA-collagen for the last frame at the end of their relaxation. A gray pixel at (i, j) point indicates that residues i and j form same amount of H-bonds in pure PVA and PVA-collagen ($\overline{H_{IJ\,\mathrm{PVA}}} - \overline{H_{IJ\,\mathrm{PVA\text{-}Col}}} = 0$); a black pixel indicates a H-bond in PVA-collagen but not in pure PVA ($\overline{H_{IJ\,\mathrm{PVA}}} - \overline{H_{IJ\,\mathrm{PVA\text{-}Col}}} = -1$); and a white pixel indicates a H-bond in pure PVA but not in PVA-collagen ($\overline{H_{IJ\,\mathrm{PVA}}} - \overline{H_{IJ\,\mathrm{PVA\text{-}Col}}} = 1$). An area is magnified for better representation. (f) Figure depicting relaxed PVA and relaxed PVA-collagen at the end of their relaxation, with end-to-end distance indicated. CHARMM, Chemistry at HARvard Macromolecular Mechanics; FF, force field.

simulations at different temperatures to test the thermal stability of the molecules. The molecules were allowed to relax until their end-to-end distance stabilized from shrinking. Various timesteps were used for numerical stability, beginning with a timestep of 0.2 fs for a duration of 0.008 ns, as the polymer chain was initially far from its equilibrium and had high velocities. The timestep was increased to 1 fs for 4 ns and then 2 fs for the remaining portion of the simulation. For PVA-collagen's relaxation, the simulation started with the timestep of 1 fs and then 2 fs for the remaining portion. Most of the simulation time is used to simulate how PVA starts with a straight chain and folds into a fully relaxed structure. We were aware of the coarse-grained model and back mapping algorithm that can accelerate the folding process of the large polymer molecule.[36,37] However, we did not use them because the coarse-grained models were not fully verified for both collagen and PVA together and could cause possible mistakes during the coarse-graining and back mapping process. We computed and monitored the root-mean-square deviation (RMSD) of the coordinates of all the atoms during the relaxation of PVA and PVA-collagen molecules to make sure that they are fully relaxed at room temperature (see Figures S1–S2 in Supplementary material).

Several tests were conducted on the relaxed molecules of PVA and PVA-collagen at different temperatures. The molecules were put under different temperatures, with the rest of the parameters the same, and further relaxed. Temperatures of 360 K, 420 K, and 480 K were controlled by means of temperature reassignment and tested to study the structure–mechanical features of the molecules at higher temperatures. The tests were all run for 3.6 ns, with a timestep of 2 fs.

In-water simulations were carried out in an NPT ensemble with constant temperature (T) and pressure ($P = 1$ atm) controlled by a Langevin thermostat and barostat. The simulations used a rigid bonds model by constraining all the covalent bonds between hydrogen atoms and other heavy atoms. We added a solvent box around the PVA structure with a TIP3P water model covering at least 10 Å from the protein structure. The net charge of the system was zero by adding NaCl of the overall concentration of 0.1 mol L^{-1} and adjusting the ratio of ions to neutralize the system. The test molecules were enclosed at the center of the water boxes, with dimensions of 180 × 100 × 110 $Å^3$ for PVA and 250 × 141 × 135 $Å^3$ for PVA-collagen. We applied periodic boundary conditions to all the *xyz* directions during the simulation. The in-water relaxation took 3.6 ns, with each timestep of 2 fs, with the structure relaxation confirmed by RMSD of the coordinates of all the atoms within the solute (see Figures S3–S4 in Supplementary material).

Steered molecular dynamics

The carbon atoms of the unit at the end of the PVA chain were pulled using steered MD (SMD) with a constant velocity, whereas the carbon atoms of the unit at the other end of the rest chains were fixed, as shown in **Figure 3**a. The pulling force was recorded versus the position. The timestep used during SMD is 1 fs for numerical stability. The molecules were tested with their temperature maintained at 300 K. The simulations were carried out at different constant pulling velocities of 0.0025, 0.005, 0.025, 0.05 $Åps^{-1}$.

Visualization and data plotting

Visual molecular dynamics (VMD) was used for post-processing of the MD simulation results. It was used to visualize and render molecular structures by going through each frame of the simulation animation and rendering every atom and bond. We developed our TCL scripts in VMD to calculate the number of hydrogen bonds (H-bonds) between any two residues i and j (given by H_{ij}). By going through all the atom pairs eligible to be donor/acceptor, a H-bond is added to H_{ij} if the donor–acceptor distance is smaller than 3.5 Å and the donor–hydrogen–acceptor angle is smaller than 35 degrees. We computed the matrix $\overline{H_{ij}}$ for the last frame at the end of a test simulation. We compared the difference of the H-bond patterns of pure PVA ($\overline{H_{ij}}_{\mathrm{PVA}}$) and PVA folded with collagen molecule ($\overline{H_{ij}}_{\mathrm{PVA\text{-}Col}}$) by $\overline{H_{ij}}_{\mathrm{PVA}} - \overline{H_{ij}}_{\mathrm{PVA\text{-}Col}}$ and plotted the positive value (for H-bonds only in PVA), zero, and negative value (for H-bonds only in PVA folded with collagen) by pixel of different colors (i.e., Figures 2e, 3c, 4a, and 5c). Using TCL scripts, VMD was used to calculate the number of H-bonds between any two residues (illustrated in Figure 2e), measure the dihedral angle between the two neighboring residues (illustrated in Figure 2c) and end-to-end distance (illustrated in **Figure 4**c), and more. Octave was used to visualize the data generated as the results of TCL scripts in VMD.

Results and discussion

We used fully atomistic molecular dynamics to relax a fully extended PVA chain consisting of 1000 residues at 300 K (Figure 2a) for a total of around 20 ns. It was shown that the molecule folds quickly into a relaxed structure composed of random coils and chain segments in parallel. This molecular structure was fully relaxed at the end of the simulation with each PVA residue stabilized by H-bonds with its neighbors. We verified the relaxation of the molecular structure by confirming no further change in RMSD and end-to-end distance, suggesting that the relaxed structure is much more energy-favored than the initially straight chain. In comparison, we equilibrated the PVA chain together with a folded tropocollagen molecule (see the section "Methods" for details of its sequence and crystal structure), by placing the N-terminus of the collagen close to the one end of the PVA chain before relaxation (Figure 2b). The relaxation took significantly longer for about 50 ns. It was shown that the PVA-collagen had a different molecular structure from the pure PVA, as it had one dimension much larger than the other two dimensions and the chain folded into serially connected hairpins in a periodic form. To better understand the difference in structure, we computed the dihedral angle of any consecutive four carbon atoms (ψ, with the backbone of two consequent PVA residues as schematically plotted

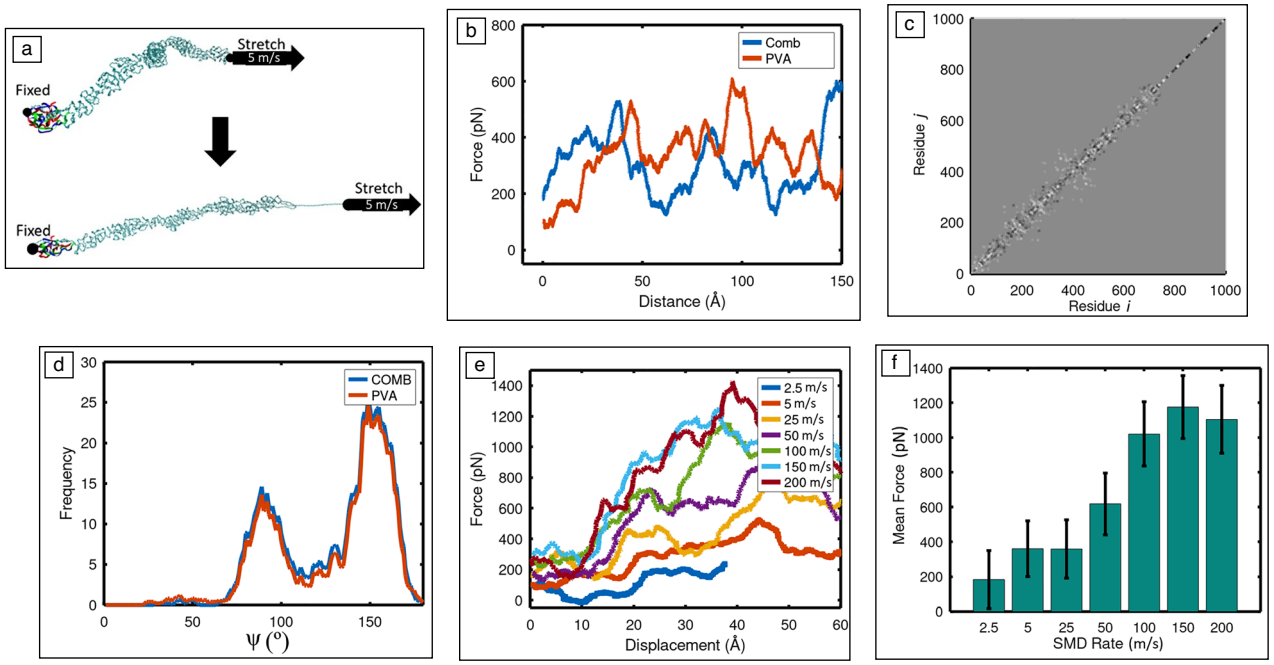

Figure 3. The results from stretching the relaxed molecules of PVA and PVA-collagen. (a) Figure depicting the stretching process of a molecule of PVA-collagen, with one end fixed whereas the other end is stretched with the desired speed. (b) The force–displacement graph of stretching PVA and PVA-collagen in vacuum, at 0.05 Åps^{-1}. (c) The hydrogen bonding graph of PVA and PVA-collagen for their structures after stretching by 30 nm. (d) The dihedral angle histogram of PVA and PVA-collagen for their structures after stretching. (e) The force–displacement graph of stretching PVA, with different pulling speeds. (f) The strength of pure PVA, defined by the average pulling force from the displacement range of 30 Å to 37.3 Å of the force–displacement curves obtained from different pulling speeds; SMD, steered molecular dynamics.

in Figure 2b). ψ measures the angle between two planes: the first three carbon atoms define a plane that includes the backbone of the previous residue (first two bonded carbon atoms) and the connecting bond between two residues, and the last three carbon atoms define another plane that includes the connecting bond between two residues and the backbone of the current residue. ψ quantifies the bent geometry at the single PVA residue. A small ψ means the two planes are folded and nearly closed, like a clamshell, and ψ ~ 180° means the two planes are open, similar to the initially straight conformation. Figure 2c summarizes ψ of each PVA backbone within pure PVA and PVA-collagen. It was shown that only few residues have ψ < 50°, corresponding to the severely bended regions that take place at the coiled region of the hairpins. The histogram of ψ (Figure 2d) showed that the PVA-collagen has slightly fewer residues with a bended conformation ψ < 120° than the pure PVA, and PVA-collagen had more residues with ψ > 120°, suggesting that there were slightly more residues in the straight region of the hairpins in PVA-collagen. The difference in these structures suggested that a PVA chain folded into a more ordered and less entangled structure by interacting with the collagen molecule. It was observed that the residues in the straight segments in parallel form a H-bonds network, in analogy to the beta-sheet structure in peptide that has a synergistic effect in stabilizing the protein structure.[38] The observation agreed with the experimental results that PVA chains fold into a more crystal structure at the collagen interface.[17]

We studied the interface between PVA and collagen by analyzing the pattern of the H-bonds formed between the residues within each collagen chain and the PVA residues during the relaxation. The 1000-residue PVA chain only forms H-bonds with collagen within the first 53 residues, while the collagen chains had their beginning, middle, and end bonded to PVA periodically. This could be because of the rigidity and periodic structure of collagen. We have also conducted experiments with different lengths of PVA, choosing one with 100 residues and one with 500 residues. The dihedral angle results after they were relaxed in vacuum were very similar to the dihedral angle results with the 1000-residue PVA chain, both with PVA-collagen having higher peaks, suggesting that collagen has similar effects on PVA even with different chain lengths.

To understand the effect of collagen on the hydrogen bonding (H-bonding) pattern of the PVA, we compared the difference between the H-bonding matrix H_{ij} for the amount of H-bonds between any two PVA residues (residue i and j; see the section "Methods" for the criterion of counting H-bonds) at the end of the relaxation for pure PVA and PVA-collagen molecule and plotted the difference by a 1000 × 1000 pixel tricolored heat map in Figure 2e. A gray pixel at (i, j) point indicates that residues i and j form the same number of

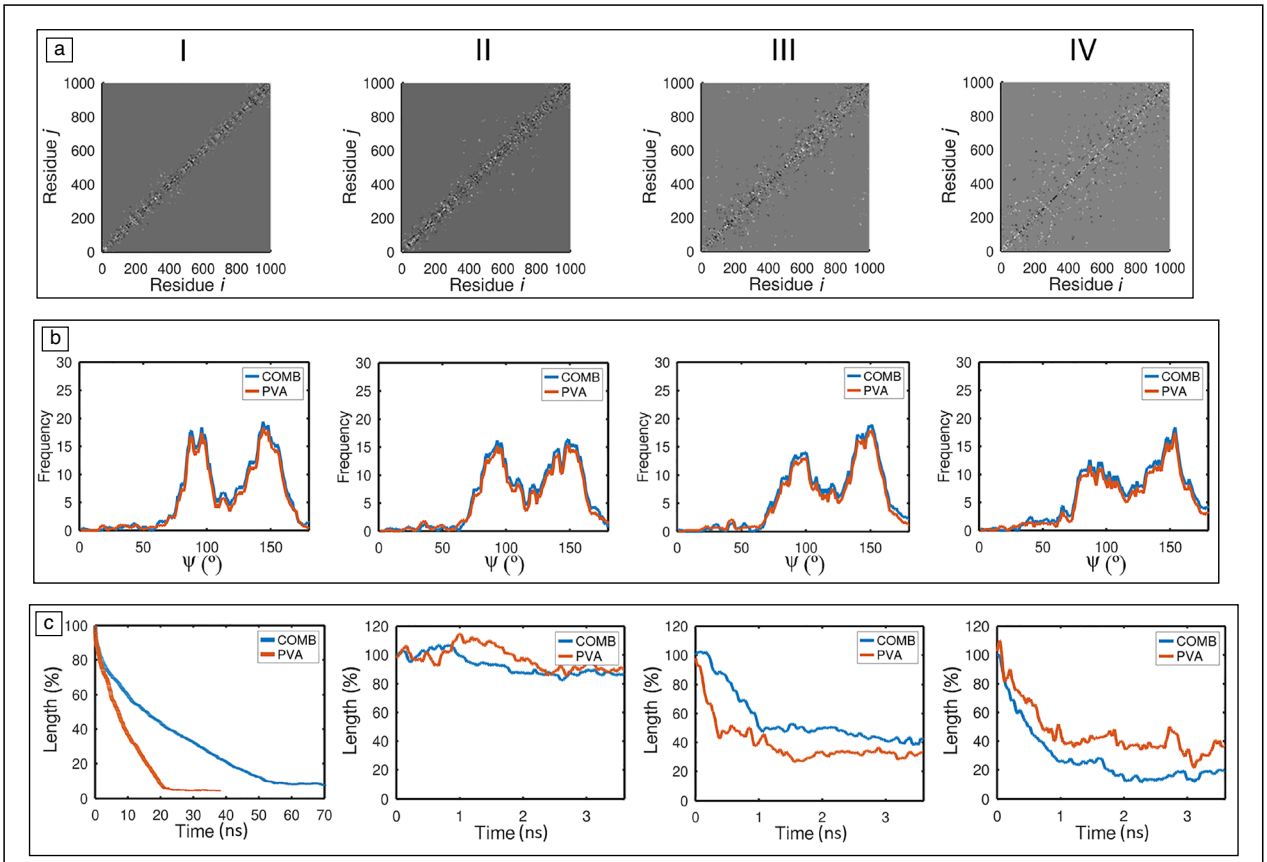

Figure 4. The results of relaxed PVA and PVA-collagen at various temperatures. Column I contains the results at 300 K; column II contains the results at 360 K; column III contains the results for at 420 K; column IV contains the results at 480 K. (a) The hydrogen bonding graph for relaxed PVA and PVA-collagen at of the end of their relaxation at defined temperatures. (b) The dihedral angle graph for relaxed PVA and PVA-collagen at the end of their relaxation at defined temperatures, ordered by the angle in degrees. (c) Column I shows the end-to-end distance of the PVA segment as PVA and PVA-collagen go from straight chain, which is a length of 2597.6 Å and 2591.1 Å, respectively, to fully relaxed, which is a length of 117.6 Å (4.53% of original length) and 195.8 Å (7.56% of original length), respectively, at 300 K; columns II, III, and IV show the further relaxation of PVA and PVA-collagen, which were prerelaxed at 300 K to the lengths of 117.6 Å and 195.8 Å, respectively, at defined temperatures, 360 K, 420 K, and 480 K, respectively.

H-bonds in pure PVA and PVA-collagen ($\overline{H_{ij}}_{\mathrm{PVA}} - \overline{H_{ij}}_{\mathrm{PVA\text{-}Col}} = 0$); a black pixel indicates a H-bond in PVA-collagen but not in pure PVA ($\overline{H_{ij}}_{\mathrm{PVA}} - \overline{H_{ij}}_{\mathrm{PVA\text{-}Col}} = -1$), and a white pixel indicates a H-bond in pure PVA but not in PVA-collagen ($\overline{H_{ij}}_{\mathrm{PVA}} - \overline{H_{ij}}_{\mathrm{PVA\text{-}Col}} = 1$). It was clearly shown that white dots tended to distribute further away from the diagonal, suggesting that pure PVA had more H-bonds between hydroxyl groups of the residues that were further away in sequence, whereas the black dots tended to cluster around the diagonal, suggesting that PVA-collagen had more H-bonds form between the neighboring residues. The H-bond pattern, combining with the ψ distribution, suggested that the PVA-collagen folded into a more compact and ordered structure. To estimate and compare the rigidity of the folded structure, we measured the end-to-end distance of the folded chain (R) and compute the persistence length by a worm-like-chain model for $L_0 >> p$, given by

$$P = \frac{R^2}{2L_0}, \qquad 1$$

where $L_0 = 2594$ Å was the contour length as the initial length of the fully extended PVA molecule. As shown in Figure 2f, pure PVA had an end-to-end distance of around 124.85 ± 5.92 Å and a persistence length of around 3.01 ± 0.29 Å, which was a little shorter than the persistence length of the polypeptide chain (~4 Å)[39] and was about the length of 1.16 PVA residues, whereas the PVA segment of combined PVA-collagen had an end-to-end distance of around 196.69 ± 5.12 Å and a persistence length of around 7.46 ± 0.36 Å, which was a little longer than the persistence length of the polypeptide chain and was about the length of 2.88 PVA residues. The persistence length results have undergone an unpaired T-test with the two-tailed P value less than 0.001, meaning their differences are statistically significant. The higher persistence length of

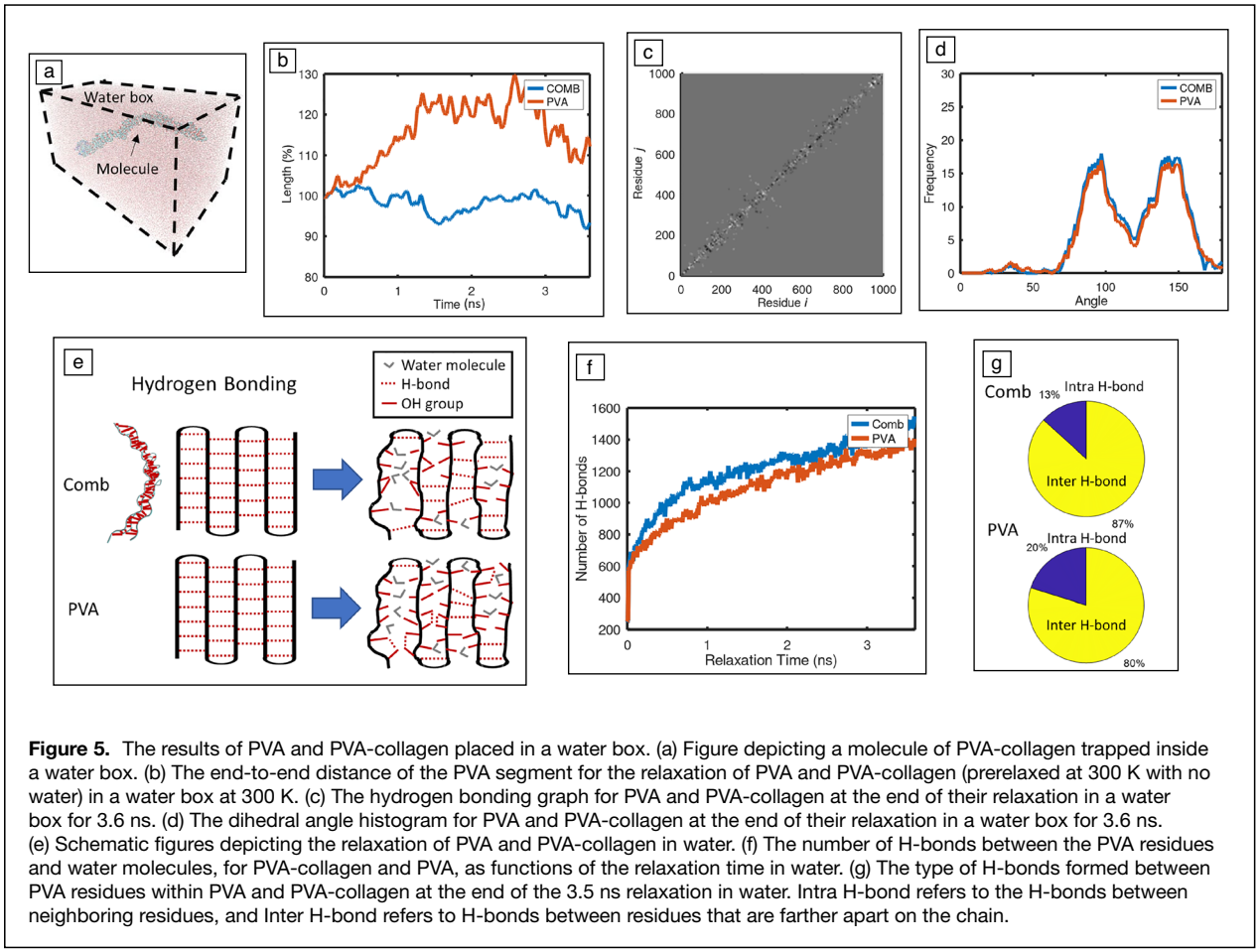

Figure 5. The results of PVA and PVA-collagen placed in a water box. (a) Figure depicting a molecule of PVA-collagen trapped inside a water box. (b) The end-to-end distance of the PVA segment for the relaxation of PVA and PVA-collagen (prerelaxed at 300 K with no water) in a water box at 300 K. (c) The hydrogen bonding graph for PVA and PVA-collagen at the end of their relaxation in a water box for 3.6 ns. (d) The dihedral angle histogram for PVA and PVA-collagen at the end of their relaxation in a water box for 3.6 ns. (e) Schematic figures depicting the relaxation of PVA and PVA-collagen in water. (f) The number of H-bonds between the PVA residues and water molecules, for PVA-collagen and PVA, as functions of the relaxation time in water. (g) The type of H-bonds formed between PVA residues within PVA and PVA-collagen at the end of the 3.5 ns relaxation in water. Intra H-bond refers to the H-bonds between neighboring residues, and Inter H-bond refers to H-bonds between residues that are farther apart on the chain.

PVA-collagen further suggested that the overall folded and curved PVA-collagen molecule appeared to be more rigid in bending and difficult to be deformed before the unfolding of each individual hairpin occurs, as shown in Figure 3a.

To understand how the difference in conformation and distribution of H-bonding caused the difference in molecular mechanics, we directly unfolded the PVA structures by fixing one end and using SMD to apply loading force to the other end with a constant velocity (0.05 Åps^{-1}) and recorded the force–displacement relationship as shown in Figure 3a. Figure 3b shows the force–displacement plot of PVA and PVA-collagen during stretching. It could be observed that during the initial phase, PVA-collagen needed more force for displacement than PVA. This showed that with the added collagen, the structure was stronger and could withstand more force before plastic (irreversible) deformation occurred (i.e., a higher Young's modulus). The material was stretched for 6 ns, for a distance of 30 nm and we analyzed and compared the structures after stretching. As shown in Figure 3c, we found both the PVA and PVA-collagen molecule unfold from the pulling end, with H-bonds being lost after residue 800 (closer to the pulling end). Moreover, we found consistent results in the H-bonding data and dihedral angle data in the stretched molecules as the unstretched molecules, with PVA-collagen still forming H-bonds between hydroxyl groups that were closer in sequence (Figure 3c) and having larger peaks in dihedral angle frequencies (Figure 3d), meaning that while the stretching force partially unfolded the molecular structure, it did not alter the molecular structure of the largely folded region, and the PVA-collagen molecule, after being partially unfolded, was still more ordered than the pure PVA. We changed the pulling speed to understand how the difference in mechanics may vary with different loading rates. As shown in Figure 3e and f, there existed a trend that as pulling speed increases, the pulling force also increased. While this was only tested on PVA, the same trend was expected on PVA-collagen, because, as seen in Figure 3a, the majority of stretching (unfolding) happened on the PVA part, not the collagen or the PVA-collagen interface. Overall, the results suggested that the PVA-collagen molecule could better resist a faster pull or impact by exerting a larger force against the deformation.

To understand how the materials behave under higher temperatures, we then tested the PVA and PVA-collagen molecules at 360 K, 420 K, and 480 K, allowing the molecule, which was pre-relaxed at 300 K, to further relax for a few nanoseconds. We computed and summarized the H-bonding data and dihedral angle data at the end of the relaxation in Figure 4a and b for comparison. It was shown that PVA-collagen exhibits

consistent patterns (as previously mentioned) in H-bonding data and dihedral angle data that suggested it to still be more crystallized than PVA under higher temperatures. Figure 4c shows the end-to-end distance of the PVA segment of the PVA and combined PVA-collagen during further relaxation at different temperatures. The graphs showed that once the molecules were heated up, the end-to-end distance gradually decreased, suggesting a smaller persistence length for both molecules. At 360 K, a temperature common for fresh hot food, combined PVA-collagen appeared to fluctuate less than pure PVA, retaining around 85% of their original length at 300 K, whereas PVA-collagen had end-to-end length (169.29 Å) still much longer than that of the PVA (106.36 Å). At 420 K, combined PVA-collagen still appeared to fluctuate less and slower than PVA, as it had a flatter slope of decline and retained more of its length at the end (83.05 Å), around 40% of its original length at 300 K, versus pure PVA's steeper decline and a lower length (40.16 Å) of only around 35% of its original length at 300 K; however, at this stage, neither material was good for real-world usage as plastics that need to hold its shape. It could, however, possibly serve as heat shrinkable film for packaging, but this is yet to be explored. At even higher temperatures of 480 K, which is beyond the glass-transition temperature of PVA and most plastics, combined PVA-collagen appeared to shrink more and faster than pure PVA. It could be understood that PVA-collagen remained more rigid at 360 K and 420 K, but softer at 480 K, which may be a useful character for manufacturing purposes (e.g., molding, 3D printing, etc.).

The mechanical properties of dry combined PVA-collagen structure are theoretically stronger than that of the pure PVA in room temperature and slightly higher temperatures. To understand if adding collagen can alleviate one of the main downsides of pure PVA, its inability to withstand humidity, we surrounded the molecule with a water box (**Figure 5**a) as described in the section "Methods." After being allowed to relax for 3.6 ns, the material again generated consistent H-bonding data and dihedral angle data (Figure 5c, d), suggesting PVA-collagen was more ordered than pure PVA molecule. The end-to-end distance for the PVA segment of PVA-collagen, as shown in Figure 5b, fluctuated significantly less than pure PVA. It shrank a maximum of around 8% whereas PVA expanded a maximum of around 30 percent. We thus obtained the persistence length of 6.98 ± 0.87 Å for PVA-collagen and 3.06 ± 0.40 Å for pure PVA in water using Equation 1, suggesting PVA-collagen remained much stiffer in water and continued to have more ordered structures. The persistence length results have undergone an unpaired T-test with the two-tailed P value less than 0.001, suggesting their differences are statistically significant.

We have computed the number of hydrogen bonds between PVA or PVA-collagen and water molecules as they relax in water. As shown in Figure 5f, we found that PVA-collagen has slightly more hydrogen bonds, suggesting that its structure has more water molecules within, as illustrated in Figure 5e. More H-bonds with water also means less H-bonds between PVA residues, because the 1000-residue PVA chain can only generate a maximum of ~2000 H-bonds, because a hydroxyl group can play both the role of donor and acceptor. Although pure PVA has more H-bonds between its residues, it also has more H-bonds between its neighbors, with 20% of the H-bonds between nearest neighbors with only a single residue away on the chain. PVA-collagen has less H-bonds between nearest neighbors (13%), with more bonds between residues that are farther off on the chain (Figure 5g), indicating that they are more responsible to the mechanical stability of the structure.

It is noted that the 3.6 ns equilibrium may only provide a quasi-stable structure to qualitatively show the effect of water molecules. The decaying function $N = N_0(1 - e^{-\frac{t}{t_0}})$ enables us to fit the data in Figure 5f and estimate that the full equilibration of the molecules requires around ~100 ns of simulation, which needs improved algorithm or faster computers.

Conclusion

Using molecular dynamics simulation, the nanomechanics and interface properties with other bioparticles, in this case collagen, of folded PVA structure could be obtained. The PVA structure folded at room temperature was stabilized by randomly formed H-bonds between hydroxyl groups, but there was a lack of ordered structure, making the structure susceptible to unfolding with temperature fluctuation and interaction with water molecules; however, most existing research on PVA were (1) building PVA with complex compounds that were likely to hinder the material's degradation;[40] (2) seeking very specific applications of the material, mostly in medical areas, that required special characteristics, like biocompatibility or extreme durability,[41–43] which made little contribution to the possibility of using PVA as a plastic replacement. We proceeded to study the mixture of PVA and collagen and investigate how the PVA structure and mechanics are stabilized by forming an interface with collagen.

Our results demonstrated that the structure and mechanics of a synthetic polymer can be tuned by a tiny amount of a natural polymer at the molecular interface. We provided the mechanism of the mechanical advantages as experimentally observed, in that PVA-collagen had a different molecular structure from the pure PVA, as it had one dimension much larger than the other two dimensions and the chain folded into serially connected hairpins that were composed of periodic segments. It shed light on identifying a way to improve the mechanics of biodegradable materials without adding much cost, which is crucial to substitute conventional plastics for environmental safety.

PVA-collagen was shown to be consistently more ordered in the various H-bonding graphs and dihedral angle graphs that all shared the same patterns of PVA-collagen bonding between hydroxyl groups that are closer together on the chain and higher peaks and higher proportion of larger dihedral angles. Combined PVA-collagen was stronger than pure PVA in dry, room temperature, or slightly higher temperatures, but this alone would not solve PVA's major disadvantage, its inability to withstand water. PVA-collagen

was especially better performing in water or high humidity, showing significantly lower fluctuation in length and indication of more order in H-bonding and dihedral angle data. Moreover, we observed that PVA-collagen and PVA both shrank significantly in higher temperatures, and it could be explored to utilize the property, possibly creating a degradable heat shrinkable packaging in future experiments.

This study provides insights into mixing PVA with collagen with the aim of constructing a biodegradable composite material with a higher capacity to withstand heat and humidity, enabling its durability in use while still being friendly to the environment, setting the basics to its potential use in replacing plastic.

Our computational model provides the molecular mechanism to explain how PVA-collagen is mechanically stronger than pure PVA, as what has been observed by the mechanics of hydrogels,[19–21] but there remains crucial work needed before its replacement for plastics. For example, the degradability of the PVA-collagen is yet to be fully tested because the simulations are limited to the time scale of nanoseconds and can't simulate the days or even weeks it would take for the material to break down. However, our combined material is, by number of atoms, around 90% PVA, which is easy to degrade, and the rest 10% made of collagen, which is a common and biodegradable material. We project that the H-bonds holding PVA and collagen together can degrade in natural environments, and then PVA and collagen will degrade and be less harmful than traditional plastic in nature.

Acknowledgments

Z.Q. acknowledges the National Science Foundation CAREER Grant (Award No. 2145392) and Syracuse University CUSE (II-35-2020) for financial support.

Data availability

The data sets generated and codes used during the current study are available from the corresponding author on reasonable request.

Conflict of interest

On behalf of all authors, the corresponding author states that there is no relevant financial or nonfinancial interests to disclose. On behalf of all authors, the corresponding author states that there is no conflict of interest.

Open access

Supplementary information

The online version contains supplementary material available at https://doi.org/10.1557/s43577-022-00416-0.

References

1. K.L. Law, N. Starr, T.R. Siegler, J.R. Jambeck, N.J. Mallos, G.H. Leonard, *Sci. Adv.* **6**(44), eabd0288 (2020). https://doi.org/10.1126/sciadv.abd0288
2. T. O'Brine, R.C. Thompson, *Mar. Pollut. Bull.* **60**, 2279 (2010). https://doi.org/10.1016/j.marpolbul.2010.08.005
3. M.R. Gregory, A.L. Andrady, "Plastics in the Marine Environment," in *Plastics and the Environment* (Wiley, Hoboken, 2004), Part 3, p. 379
4. D.K.A. Barnes, *Nature* **416**, 808 (2002). https://doi.org/10.1038/416808a
5. D.K.A. Barnes, P. Milner, *Mar. Biol.* **146**, 815 (2005). https://doi.org/10.1007/s00227-004-1474-8
6. R.L. Reddy, V.S. Reddy, G.A. Gupta, *Int. J. Emerg. Technol. Adv. Eng.* **3**, 76 (2013)
7. R.O. Ritchie, *Nat. Mater.* **10**, 817 (2011). https://doi.org/10.1038/nmat3115
8. J.A. Rogers, T. Someya, Y. Huang, *Science* **327**(5793), 1603 (2010)
9. J.-Y. Sun, X. Zhao, W.R.K. Illeperuma, O. Chaudhuri, K.H. Oh, D.J. Mooney, J.J. Vlassak, Z. Suo, *Nature* **489**, 133 (2012). https://doi.org/10.1038/nature11409
10. J. Jancar, J.F. Douglas, F.W. Starr, S.K. Kumar, P. Cassagnau, A.J. Lesser, S.S. Sternstein, M.J. Buehler, *Polymer* (Guildford) **51**(15), 3321 (2010)
11. J.P. Gong, Y. Katsuyama, T. Kurokawa, Y. Osada, *Adv. Mater.* **15**, 1155 (2003). https://doi.org/10.1002/adma.200304907
12. V.G. Kadajji, G.V. Betageri, *Polymers* (Basel) **3**, 1972 (2011)
13. F.M. Veronese, G. Pasut, *Drug Discov. Today* **10**, 1451 (2005)
14. E. Ruel-Gariépy, J.C. Leroux, *Eur. J. Pharm. Biopharm.* **58**, 409 (2004)
15. T. Ackbarow, X. Chen, S. Keten, M.J. Buehler, *Proc. Natl. Acad. Sci. U.S.A* **104**, 16410 (2007). https://doi.org/10.1073/pnas.0705759104
16. S. Keten, Z.P. Xu, B. Ihle, M.J. Buehler, *Nat. Mater.* **9**, 359 (2010). https://doi.org/10.1038/NMAT2704
17. J. Liu, S. Lin, X. Liu, Z. Qin, Y. Yang, J. Zang, X. Zhao, *Nat. Commun.* **11**, 1071 (2020). https://doi.org/10.1038/s41467-020-14871-3
18. C.C. DeMerlis, D.R. Schoneker, *Food Chem. Toxicol.* **41**, 319 (2003). https://doi.org/10.1016/S0278-6915(02)00258-2
19. Z. Peng, Z. Li, F. Zhang, X. Peng, *J. Macromol. Sci. Part B Phys.* **51**(10), 1934 (2012). https://doi.org/10.1080/00222348.2012.660060
20. X. Wu, W. Li, K. Chen, D. Zhang, L. Xu, X. Yang, *Mater. Today Commun.* **21**, 100792 (2019). https://doi.org/10.1016/j.mtcomm.2019.100702
21. Z. Bai, T. Wang, X. Zheng, Y. Huang, Y. Chn, W. Dan, *Polym. Eng. Sci.* **61**(1), 278 (2021). https://doi.org/10.1002/pen.25574
22. F. Bachtiger, T.R. Congdon, C. Stubbs, M.I. Gibson, G.C. Sosso, *Nat. Commun.* **12**, 1323 (2021). https://doi.org/10.1038/s41467-021-21717-z
23. K. Vanommeslaeghe, E. Hatcher, C. Acharya, S. Kundu, S. Zhong, J. Shim, E. Darian, O. Guvench, P. Lopes, I. Vorobyov, A.D. MacKerell Jr., *J. Comput. Chem.* **31**(4), 671 (2010). https://doi.org/10.1002/jcc.21367
24. B.R. Brooks, R.E. Bruccoleri, B.D. Olafson, D.J. States, S. Swaminathan, M. Karplus, *J. Comput. Chem.* **4**(2), 187 (1983). https://doi.org/10.1002/jcc.540040211
25. T. Lazaridis, M. Karplus, *Proteins Struct. Funct. Bioinform.* **35**(2), 133 (1999). https://doi.org/10.1002/(Sici)1097-0134(19990501)35:2%3c133::Aid-Prot1%3e3.0.Co;2-N
26. A.D. MacKerell Jr., D. Bashford, M. Bellott, R.L. Dunbrack Jr., J.D. Evanseck, M.J. Field, S. Fischer, J. Gao, H. Guo, S. Ha, D. Joseph-McCarthy, L. Kuchnir, K. Kuczera, F.T.K. Lau, C. Mattos, S. Michnick, T. Ngo, D.T. Nguyen, B. Prodhom, W.E. Reiher, B. Roux, M. Schlenkrich, J.C. Smith, R. Stote, J. Straub, M. Watanabe, M. Wiórkiewicz-Kuczera, D. Yin, M. Karplus, *J. Phys. Chem. B* **102**(18), 3586 (1998). https://doi.org/10.1021/jp973084f
27. P.E. Marszalek, H. Lu, H. Li, M. Carrion-Vazquez, A.F. Oberhauser, K. Schulten, J.M. Fernandez, *Nature* **402**, 100 (1999). https://doi.org/10.1038/47083
28. J. Jumper, R. Evans, A. Pritzel, T. Green, M. Figurnov, O. Ronneberger, K. Tunyasuvunakool, R. Bates, A. Žídek, A. Potapenko, A. Bridgland, C. Meyer, S.A.A. Kohl, A.J. Ballard, A. Cowie, B. Romera-Paredes, S. Nikolov, R. Jain, J. Adler, T. Back, S. Petersen, D. Reiman, E. Clancy, M. Zielinski, M. Steinegger, M. Pacholska, T. Berghammer, S. Bodenstein, D. Silver, O. Vinyals, A.W. Senior, K. Kavukcuoglu, P. Kohli, D. Hassabis, *Nature* **596**, 583 (2021). https://doi.org/10.1038/s41586-021-03819-2
29. Z. Qin, L. Wu, H. Sun, S. Huo, T. Ma, E. Lim, P.-Y. Chen, B. Marelli, M.J. Buehler, *Extreme Mech. Lett.* **36**, 100652 (2020). https://doi.org/10.1016/j.eml.2020.100652
30. S.J. Marrink, D.P. Tieleman, *Chem. Soc. Rev.* **42**, 6801 (2013). https://doi.org/10.1039/c3cs60093a
31. R. Jack, D. Sen, M.J. Buehler, *J. Comput. Theor. Nanosci.* **7**, 354 (2010). https://doi.org/10.1166/jctn.2010.1366

32. A. Gautieri, S. Vesentini, A. Redaelli, M.J. Buehler, *Nano Lett.* **11**, 757 (2011). https://doi.org/10.1021/nl103943u
33. J.C. Phillips, D.J. Hardy, J.D.C. Maia, J.E. Stone, J.V. Ribeiro, R.C. Bernardi, R. Buch, G. Fiorin, J. Hénin, W. Jang, R. McGreevy, M.C.R. Melo, B.K. Radak, R.D. Skeel, A. Singharoy, Y. Wang, B. Roux, A. Aksimentiev, Z. Luthey-Schulten, L.V. Kalé, K. Schulten, C. Chipot, E. Tajkhorshid, *J. Chem. Phys.* **153**, 044130 (2020). https://doi.org/10.1063/5.0014475
34. J. Liu, S. Lin, X. Liu, Z. Qin, Y. Yang, J. Zang, X. Zhao, *Nat. Commun.* **11**, 1071 (2020). https://doi.org/10.1038/S41467-020-14871-3
35. K. Vanommeslaeghe, E.P. Raman, A.D. MacKerell Jr., *J. Chem. Inf. Model.* **52**(12), 3155 (2012). https://doi.org/10.1021/ci3003649
36. Y.K. Choi, S.-J. Park, S. Park, S. Kim, N.R. Kern, J. Lee, W. Im, *J. Chem. Theory Comput.* **17**(4), 2431 (2021). https://doi.org/10.1021/acs.jctc.1c00169
37. P. Eastman, J. Swails, J.D. Chodera, R.T. McGibbon, Y. Zhao, K.A. Beauchamp, L.-P. Wang, A.C. Simmonett, M.P. Harrigan, C.D. Stern, R.P. Wiewiora, B.R. Brooks, V.S. Pande, *PLoS Comput. Biol.* **13**(7), e1005659 (2017). https://doi.org/10.1371/journal.pcbi.1005659
38. K. Tsemekhman, L. Goldschmidt, D. Eisenberg, D. Baker, *Protein Sci.* **16**, 761 (2007). https://doi.org/10.1110/ps.062609607
39. S. Keten, M.J. Buehler, *Phys. Rev. Lett.* **100**, 198301 (2008). https://doi.org/10.1103/PhysRevLett.100.198301
40. V.C. Li, S. Wang, C. Wu, *ACI Mater. J.* **98**(6), 483 (2001). https://doi.org/10.14359/10851
41. Z. Wu, B. Kong, R. Liu, W. Sun, S. Mi, *Nanomaterials* (Basel) **8**(2), 124 (2018). https://doi.org/10.3390/nano8020124
42. M. Kokabi, M. Sirousazar, Z.M. Hassan, *Eur. Polym. J.* **43**, 773 (2007). https://doi.org/10.1016/j.eurpolymj.2006.11.030
43. S. Jiang, S. Liu, W. Feng, *J. Mech. Behav. Biomed. Mater.* **4**, 1228 (2011). https://doi.org/10.1016/j.jmbbm.2011.04.005